INSTITUTE OF PHYSICS PUBLISHING JOURNAL OF PHYSICS A: MATHEMATICAL AND GENERAL

J. Phys. A: Math. Gen. **38** (2005) 9317–9339 doi:10.1088/0305-4470/38/42/011

A regular semiclassical approximation for the propagation of wave packets with complex trajectories

Fernando Parisio and M A M de Aguiar

Instituto de Física 'Gleb Wataghin', Universidade Estadual de Campinas, 13083-970, Campinas, SP, Brazil

Received 28 April 2005, in final form 12 September 2005
Published 5 October 2005
Online at stacks.iop.org/JPhysA/38/9317

Abstract

The semiclassical propagation of Gaussian wave packets by complex classical trajectories involves multiple contributing and noncontributing solutions interspersed by phase space caustics. Although the phase space caustics do not generally lie exactly on the relevant trajectories, they might strongly affect the semiclassical evolution depending on their proximity to them. In this paper, we derive a third-order regular semiclassical approximation which correctly accounts for the caustics and which is finite everywhere. We test the regular formula for the potential $V(x) = 1/x^2$, where the complex classical trajectories and phase space caustics can be computed analytically. We make a detailed analysis of the structure of the complex functions involved in the saddle point approximations and show how the changes in the steepest descent integration contour control both the contributing and noncontributing trajectories and the type of Airy function that appears in the regular approximation.

PACS numbers: 03.65.Sq, 03.65.Nk

1. Introduction

The study of the semiclassical propagation of wave packets plays a very important role in the understanding of the transition between classical and quantum dynamics. One of the main goals of this study is to investigate how classical dynamical ingredients enter in the semiclassical description of purely quantum properties, such as interference, tunnelling and coherence. Also important is to understand how accurate the semiclassical formulae are and for how long they remain reliable. The semiclassical propagation of wave packets is also a widely used tool in modelling a great variety of phenomena in chemistry and physics. They have been particularly important in investigations of quantum chaos [Tom91, Pro95, Sil02, Tom03, Fie03, Rib04] and molecular dynamics [Tho04, Kay05].

The basic semiclassical formula for the time evolution of wavefunctions is the so-called van Vleck propagator, which represents the semiclassical limit of the matrix element

$\langle x|\hat{K}(T)|x'\rangle = K(x, x', T)$ of the evolution operator $\hat{K}(T) = \exp\{-\mathrm{i}\hat{H}T/\hbar\}$:

$$K_{\mathrm{vv}}(x, x', T) = \frac{1}{\sqrt{2\pi\hbar}} \sum_{\text{classical paths}} \left(-\frac{\partial^2 S}{\partial x \partial x'}\right)^{-1/2} \exp\left(\frac{\mathrm{i}}{\hbar} S(x, x', T) - \frac{\mathrm{i}\pi}{4}\right). \tag{1.1}$$

The classical quantities involved in this formula are the trajectories that propagate from x' to x in the time T, together with their actions S and the properties of their neighbouring orbits, contained in the second derivative of S. The knowledge of $K_{\mathrm{vv}}(x, x', T)$ allows the semiclassical propagation of any initial state through the composition

$$\psi_{\mathrm{sc}}(x, t) = \int K_{\mathrm{vv}}(x, x', T)\psi(x', 0)\,\mathrm{d}x'. \tag{1.2}$$

However, in order to be implemented, the above expression requires the calculation of a double infinity of classical trajectories, since trajectories from x' to x have to be computed for all values of x' and all values of x. Several methods have been proposed in the past years to circumvent this difficulty, and two of them have stand out. The first method transforms the double infinity of trajectories with mixed boundary conditions (x' at time zero and x at time T) to another double infinity of trajectories with initial conditions (x' and p' at time zero). These are the so-called initial value representations (IVR). In this paper, we shall not consider IVR methods and we refer to the recent reviews in [Tho04, Kay05] for more information on the several variations of this technique, its accuracy and applications.

The second approach consists in performing the integration over x' directly using the saddle point method [Hub88, Agu05]. This eliminates the need to find trajectories for all values of x'. Instead one considers only the few values that make the exponent stationary. However, the stationary points are usually complex, and the underlying classical dynamics takes place in a complexified phase space, where both position and momentum are complex variables. The complex dynamics gives rise to the so-called noncontributing classical solutions, which correspond to saddle points that cannot be reached by a contour of integration consistent with Cauchy's integral theorem. Of course, these points must be excluded from the evaluation of semiclassical quantities and criteria based on physical reasoning have been proposed to systematically separate them from the contributing solutions [Ada89, Shu95, Shu96, Oni01]. These criteria are much simpler to apply than the direct verification of Cauchy's theorem, which, in general, is a prohibitive task. A second problem that usually appears in asymptotic evaluations of quantum propagators is that of caustics. At these points, the common second-order semiclassical expressions diverge and higher order expansions are necessary.

The purpose of this work is twofold. First, we derive an improved semiclassical expression for the propagation of wave packets that is well behaved in the vicinity of phase space caustics. Second, we present a detailed application of the complex trajectories formalism, developed in [Hub87, Hub88, Agu05], to the scattering of a Gaussian wave packet by the one-dimensional potential $V(x) = 1/x^2$. This system is analytically solvable but nontrivial, presenting both noncontributing solutions and caustics. We test our new semiclassical expression for this problem and we show that the improved formula indeed removes the incorrect peaks produced by the caustics, leading to results that are in excellent agreement with quantum calculations. The application of the new formula involves a careful analysis of the complex plane of the action function, in order to choose the correct steepest descent integration contour. The choice of contour is what controls the contributing and noncontributing trajectories and the type of Airy function that appears in the regular approximation.

This paper is organized as follows: in the next section, we briefly review the theory presented in [Agu05] and in section 3 we discuss the possible higher order expansions that must be carried out in order to avoid the spurious effects introduced by the caustics. In

section 4, we derive one particular approximation in which the corrections are totally contained in a multiplicative factor that regularizes the quadratic formula. Section 5 contains a detailed application of the formalism to the case of a Gaussian wave packet moving in the potential $V(x) = 1/x^2$ and in section 6 we summarize our conclusions.

2. Semiclassical propagation of wave packets with complex trajectories

The time evolution of a Gaussian wave packet in the coordinate representation can be written as

$$\psi(x, T) = \langle x|\hat{K}(T)|z\rangle \tag{2.1}$$

where

$$\langle x|z\rangle = \pi^{-\frac{1}{4}} b^{-\frac{1}{2}} \exp\left[-\frac{(x-q)^2}{2b^2} + \frac{\mathrm{i}}{\hbar} p(x - q/2)\right] \tag{2.2}$$

and $\hat{K}(T) = \mathrm{e}^{-\mathrm{i}\hat{H}T/\hbar}$ is the evolution operator. The canonical coherent state $|z\rangle$ is defined by the eigenvalue equation $\hat{a}|z\rangle = z|z\rangle$, where $\hat{a} = (\hat{q}/b + \mathrm{i}\hat{p}/c)/\sqrt{2}$ is the annihilation operator and $z = (q/b + \mathrm{i}p/c)/\sqrt{2}$ is complex. The real numbers q and p are the mean values of position and momentum, respectively, and the quantities $b = \sqrt{2}\Delta q$ and $c = \sqrt{2}\Delta p$ are the corresponding uncertainties [Kla85]. The right-hand side of equation (2.1) can also be interpreted as a 'mixed propagator', with a coordinate bra on the left and a coherent state ket on the right.

A semiclassical expression for the wavefunction (2.1) was recently obtained [Agu05] using the van Vleck formula

$$\langle x|\hat{K}(T)|x'\rangle_{\mathrm{vv}} = \frac{1}{b\sqrt{2\pi m_{qp}}} \exp\left(\frac{\mathrm{i}}{\hbar} S(x, x', T) - \frac{\mathrm{i}\pi}{4}\right), \tag{2.3}$$

where a sum over classical trajectories is assumed. Earlier derivations based on different assumptions can be found in [Hub87, Hub88]. In this equation, S is the action of the (real) trajectory connecting x' and x in the time T and m_{qp} is an element of the tangent matrix defined by

$$\begin{pmatrix} \frac{\delta x_T}{b} \\ \frac{\delta p_T}{c} \end{pmatrix} \equiv \begin{pmatrix} m_{qq} & m_{qp} \\ m_{pq} & m_{pp} \end{pmatrix} \begin{pmatrix} \frac{\delta x_0}{b} \\ \frac{\delta p_0}{c} \end{pmatrix}, \tag{2.4}$$

where $(\delta x_0, \delta p_0)$ are small initial deviations from the classical trajectory and $(\delta x_T, \delta p_T)$ are the corresponding final deviations in the linear approximation. The elements of m can be written in terms of the second derivatives of the action as follows:

$$\frac{\partial^2 S}{\partial {x_0}^2} = \frac{c}{b}\frac{m_{qq}}{m_{qp}}, \qquad \frac{\partial^2 S}{\partial x_0 \partial x_T} = -\frac{c}{b}\frac{1}{m_{qp}} \qquad \text{and} \qquad \frac{\partial^2 S}{\partial {x_T}^2} = \frac{c}{b}\frac{m_{pp}}{m_{qp}}. \tag{2.5}$$

A fourth relation is given by $\det(m) = 1$. The semiclassical approximation of the mixed propagator (2.1) can be calculated from

$$\langle x|\hat{K}(T)|z\rangle \approx \int \langle x|\hat{K}(T)|x'\rangle_{\mathrm{vv}} \langle x'|z\rangle \, \mathrm{d}x' \equiv \psi_{\mathrm{sc}}(x, T). \tag{2.6}$$

The evaluation of this integral by the steepest descent method yields [Agu05]

$$\psi_{\mathrm{sc}}(x, T) = \frac{1}{b^{1/2}\pi^{1/4}} \frac{1}{\sqrt{m_{qq} + \mathrm{i}m_{qp}}} \exp\left(\frac{\mathrm{i}}{\hbar} S(x, T; x_0', 0) + \frac{\mathrm{i}}{\hbar} p(x_0' - q/2) - \frac{(x_0' - q)^2}{2b^2}\right), \tag{2.7}$$

where one should sum over the, usually complex, contributing trajectories satisfying Hamilton's equations and the boundary conditions

$$\frac{x'(0)}{b} + \mathrm{i}\frac{p'(0)}{c} = \frac{q}{b} + \mathrm{i}\frac{p}{c} \qquad \text{and} \qquad x'(T) = x. \tag{2.8}$$

To get the right phase in the semiclassical propagator one must follow the phase of the pre-factor from $t = 0$ to $t = T$.

To avoid confusion with the labels x and z of the wave packet, we have used primed letters x' and p' to refer to the time evolution of the classical trajectories. In this notation, the Hamiltonian is $H = p'^2/2 + V(x')$ and a trajectory is represented by $x'(t)$ and $p'(t)$. We also define $x'(0) = x'_0$, $p'(0) = p'_0$ and $x'(T) = x'_T$.

The mixed boundary conditions equation (2.8) can be dealt with using a procedure introduced by Klauder and first applied to a nontrivial system by Adachi [Ada89] for the coherent states propagator. It consists of writing the initial phase space points as

$$x'_0 = q + w \qquad \text{and} \qquad p'_0 = p + \mathrm{i}kw, \tag{2.9}$$

where $w = \alpha + \mathrm{i}\beta$ is a complex number and $k = c/b$. The first condition in (2.8) is automatically satisfied for any value of w. Propagating the initial points (2.9) via Hamilton's equations for all w's leads to a mapping between the complex planes w and $x'_T(w)$:

$$w \longrightarrow x'_T(w), \tag{2.10}$$

where $x'_T(w)$ represents the final complex coordinate. This mapping is conformal except possibly at isolated points that can be critical points, where $\mathrm{d}x'_T(w)/\mathrm{d}w = 0$ or singular points, where $x'_T(w) \to \infty$. We will see in subsequent sections that the critical points of the mapping (2.10), which we call caustics, correspond to the locations where the semiclassical wave functions diverge, i.e., $\mathrm{d}x'_T(w)/\mathrm{d}w = 0 \Rightarrow \psi_{\mathrm{sc}} \to \infty$. In order to satisfy the second condition in (2.8), we determine the points in the w-plane for which $\mathrm{Im}[x'_T(w)] = 0$. Note that x' is now a complex variable, due to the analytic extension, but x remains as a real quantity. The sets of points obtained at the end of this process are the complex classical solutions.

Formula (2.7), the 'bare semiclassical formula', gives a good description of the quantum wavefunction [Agu05] provided we eliminate the noncontributing trajectories [Ada89, Rub95] *and* if the effect of the caustics, where the pre-factor diverges, can be neglected. A practical method to circumvent the noncontributing trajectory problem was proposed by Adachi [Ada89] and has been shown to work well in previous applications [Ada89, Rub95, Rib04, Agu05]. The divergence of the semiclassical propagator at the caustics, however, requires an improvement in the semiclassical formula beyond the quadratic approximation. In this paper, we derive such a semiclassical approximation for the mixed propagator and test it for the one-dimensional potential $V(x') = 1/x'^2$, where all complex trajectories and caustics can be determined analytically.

3. Third-order corrections

The first step to obtain a higher order semiclassical approximation for the mixed propagator is to identify which kind of expansion must be made. To do so, let us consider the following integration:

$$\int \mathrm{e}^{\frac{\mathrm{i}}{\hbar}F(x')}\,\mathrm{d}x', \tag{3.1}$$

where F has two saddle points x'_+ and x'_-, for which $F' = 0$, and one point x'_c where $F'' = 0$, which corresponds to a caustic. Indeed, a stationary phase approximation of the above

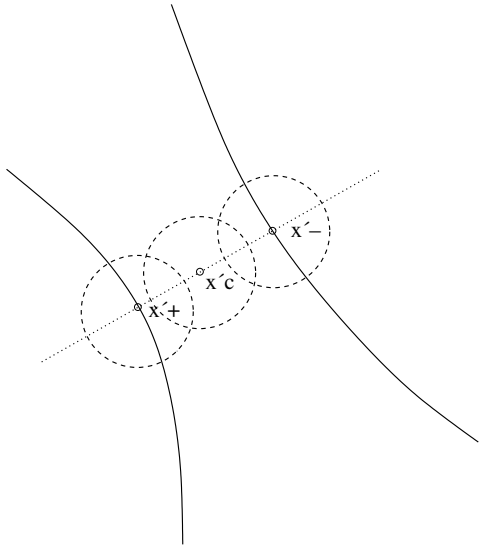

Figure 1. Illustration of saddle point families where the superposition between the relevant regions of integration can be ignored. In this case, one can add the contributions from x'_+ and x'_-.

integral with the exponent expanded to second order around the saddle points is proportional to $(F'')^{-1/2}$. Such an approximation diverges only if the saddle points coalesce at x'_c, but spurious peaks may appear if $x'_\pm$ are too close to x'_c. We denote the vicinities of x'_+ and x'_- where the contribution to the integral (3.1) is relevant by $\mathcal{D}_+$ and $\mathcal{D}_-$, respectively. Two distinct situations can occur:

(a) There is no relevant superposition between the regions $\mathcal{D}_+$ and $\mathcal{D}_-$, that is, $\mathcal{D}_+ \cap \mathcal{D}_- \approx \{\emptyset\}$. In this case, the distance between x'_+ and x'_- is big enough so that one can make expansions around each point and sum up the two contributions without significant interference or redundancy. This situation is schematically shown in figure 1. We can obtain an estimate for the validity of this procedure by looking at such an expansion in the vicinity of one of the saddle points. Let, for example, F_+ denote the expansion of $F(x)$ around x'_+:

$$F_+(x') \approx F(x'_+) + \tfrac{1}{2}F''(x'_+)(x' - x'_+)^2 + \tfrac{1}{6}F'''(x'_+)(x' - x'_+)^3. \tag{3.2}$$

Evaluating the above expression at the other saddle point and noting that F'' is small for $x_\pm$ close to x'_c, we get

$$F_+(x'_-) \approx F(x'_+) + \tfrac{1}{6}F'''(x'_+)(x'_- - x'_+)^3. \tag{3.3}$$

Therefore, if $(1/6\hbar)F'''(x'_+)(x'_- - x'_+)^3 \approx 1$ the function $\exp\{\mathrm{i}F/\hbar\}$ approximately completes one cycle as one moves from x_+ to x_- and the part of integration (3.1) corresponding to x'_+ tends to vanish in the region $x' \approx x'_-$. Under these circumstances, we can assure that the individual contributions calculated from a third-order expansion can be added. More explicitly, we should have

$$|x'_+ - x'_-| \gtrsim \left(\frac{6\hbar}{|F'''|}\right)^{1/3}. \tag{3.4}$$

(b) The other possibility occurs when $\mathcal{D}_+$ and $\mathcal{D}_-$ overlap and one cannot simply expand F for each saddle point and sum up the individual contributions because this procedure would

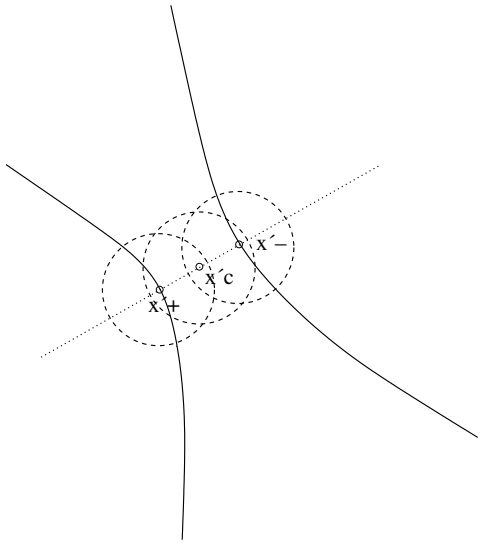

Figure 2. Illustration of saddle point families where the superposition between the relevant regions of integration cannot be ignored. In this case, summing the contributions of the critical points leads to inaccurate results.

compute twice the part referring to the region $\mathcal{D}_+ \cap \mathcal{D}_- \neq \{\emptyset\}$. One possible solution is to expand F around the caustic x'_c:

$$F(x') \approx F(x'_c) + F'(x'_c)(x' - x'_c) + \tfrac{1}{6}F'''(x'_c)(x' - x'_c)^3. \tag{3.5}$$

In this regime, the above expression can be used to get a good estimation for the integration (3.1) since it is also valid in the vicinity of x'_+ and x'_- (see figure 2). This approximation is called *transitional*, because it is valid only in the vicinity of x'_c and must be replaced by another kind of formula (typically a second-order approximation) far from this region. An example of this procedure is given by the connection formulae in WKB theory. In appendix A, we obtain the transitional approximation for the mixed propagator presented in equation (2.7).

Finally, there are third-order *uniform* approximations that are valid in all situations mentioned above. The price to be paid is a loss of accuracy in the regions away from the caustics with respect to the pure quadratic approximation [Ber67, Rib05]. We shall not consider this type of approximation in this paper.

4. Regular semiclassical approximation

The classical trajectories involved in the semiclassical propagation of wave packets do not generally have caustics. However, phase space caustics lying on nearby classical trajectories (that do not necessarily contribute to the semiclassical wavefunction) might strongly affect the semiclassical evolution depending on their proximity to them. In this section, we assume that the distance between these caustics and the contributing trajectories are not too small, so that condition (3.4) is fulfilled. This seems to be the most common situation for wave packets

projected in the coordinate or momentum representations [Hub88]. We write equation (2.6) as

$$\Psi_{\rm sc}(x,T)=\int_{-\infty}^{+\infty}\frac{{\rm e}^{-{\rm i}\pi/4}\exp\{{\rm i}F/\hbar\}}{b^{3/2}\pi^{1/4}\sqrt{2\pi m_{qp}}}\,{\rm d}x', \tag{4.1}$$

where

$$F(x,T;x',0)=S(x,T;x',0)+p(x'-q/2)+{\rm i}\hbar\frac{(x'-q)^2}{2b^2}. \tag{4.2}$$

We shall carry out a third-order expansion of F analogous to that in equation (3.2). In order to distinguish the resulting formula from the transitional or uniform approximations, we shall term it *regular* semiclassical approximation and denote it by the capital letter $\Psi_{\rm sc}$.

We expand F up to third order in the difference $(x'-x_0')$, where x_0' is a saddle point determined by

$$\frac{\rm i}{\hbar}F'\equiv\frac{\rm i}{\hbar}\frac{\partial F}{\partial x'}=\frac{\rm i}{\hbar}(p-p')-\frac{(x'-q)}{b^2}=0, \tag{4.3}$$

with

$$p'(x,x',T)=-\frac{\partial S}{\partial x'}. \tag{4.4}$$

Note that the stationary condition gives the first complex boundary condition in (2.8) with $p_0'(x,T)=p'(x,x_0',T)$. The second- and third-order derivatives are

$$\frac{\rm i}{\hbar}F''\equiv\frac{\rm i}{\hbar}\frac{\partial^2 F}{\partial x'^2}=-\frac{\rm i}{\hbar}\frac{\partial p'}{\partial x'}-\frac{1}{b^2}, \tag{4.5}$$

and

$$\frac{\rm i}{\hbar}F'''\equiv\frac{\rm i}{\hbar}\frac{\partial^3 F}{\partial x'^3}=-\frac{\rm i}{\hbar}\frac{\partial^2 p'}{\partial x'^2}. \tag{4.6}$$

Inserting

$$F\approx F(x_0')+\tfrac{1}{2}F''(x_0')(x'-x_0')^2+\tfrac{1}{6}F'''(x_0')(x'-x_0')^3 \tag{4.7}$$

into (4.1) and evaluating the pre-factor at the saddle point [Bar01] we obtain

$$\Psi_{\rm sc}(x,T)=\frac{{\rm e}^{-{\rm i}\pi/4}\exp\{{\rm i}F(x_0')/\hbar\}}{b^{3/2}\pi^{1/4}\sqrt{2\pi m_{qp}}}\int_{\mathcal{C}}\exp\left\{{\rm i}A(x'-x_0')^2+\frac{{\rm i}B}{3}(x'-x_0')^3\right\}{\rm d}x', \tag{4.8}$$

where

$$A=\frac{F''(x_0')}{2\hbar}=\frac{1}{2b^2}\left(\frac{m_{qq}+{\rm i}m_{qp}}{m_{qp}}\right)_{x_0'}, \tag{4.9}$$

and

$$B=\frac{F'''(x_0')}{2\hbar}=\frac{1}{2b^2}\frac{\partial}{\partial x'}\left(\frac{m_{qq}}{m_{qp}}\right)_{x_0'}. \tag{4.10}$$

The original integration contour (real axis) must be deformed into a new contour $\mathcal{C}$ in order to pass through the saddle point x_0' while keeping the integral (4.8) bounded. It is convenient to write

$$\frac{B}{3}(x'-x_0')^3+A(x'-x_0')^2=\frac{1}{3}[\gamma(x'-x_0')+\sigma]^3+\mu[\gamma(x'-x_0')+\sigma]+\frac{2}{3}\sigma^3, \tag{4.11}$$

with

$$\gamma=B^{1/3},\qquad \sigma=\frac{A}{B^{2/3}},\qquad \mu=-\frac{A^2}{B^{4/3}}, \tag{4.12}$$

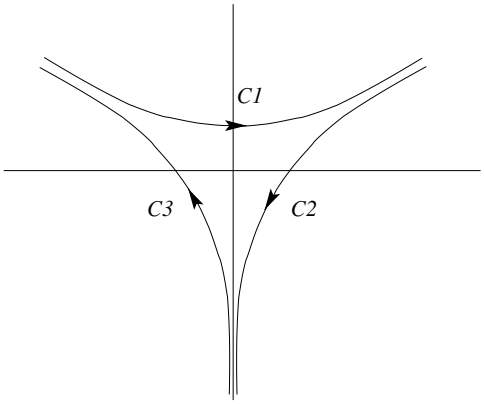

Figure 3. Possible contours for the integration of equation (4.15).

where, without loss of generality, $B^{1/3}$ stands for the principal root of $\gamma^3 = B$ (see appendix B). Rewriting the integral in (4.8) in terms of the new variable $t = \gamma(x' - x_0') + \sigma$, we obtain

$$\int_{\mathcal{C}} \exp\left\{\mathrm{i}A(x'-x_0')^2 + \frac{\mathrm{i}B}{3}(x'-x_0')^3\right\}\mathrm{d}x' = \frac{1}{B^{1/3}}\exp\left(\mathrm{i}\frac{2A^3}{3B^2}\right) I\left(-\frac{A^2}{B^{4/3}}\right), \tag{4.13}$$

with

$$I(s) \equiv \int_{\mathcal{C}} \exp\left\{\mathrm{i}\left[\frac{1}{3}t^3 + st\right]\right\}\mathrm{d}t. \tag{4.14}$$

Since I has to be bounded, the new integration contour $\mathcal{C}$ must be deformable into one of the curves $\mathcal{C}_j$ shown in figure 3. Therefore, we are lead to identify the function $I(s)$ with either the Airy function, also denoted by f_1, or one of the related functions f_2 or f_3 [Ble86]:

$$I(s) = 2\pi f_j(s) \equiv \int_{\mathcal{C}_j} \exp\left\{\mathrm{i}\left[\frac{1}{3}t^3 + st\right]\right\}\mathrm{d}t. \tag{4.15}$$

The semiclassical wavefunction becomes

$$\Psi_{\mathrm{sc}}(x,T) = \frac{\mathrm{e}^{-\mathrm{i}\pi/4}\exp\{\mathrm{i}F(x_0')/\hbar\}}{b^{3/2}\pi^{1/4}\sqrt{2\pi m_{qp}}} \times \frac{1}{B^{1/3}}\exp\left(\mathrm{i}\frac{2A^3}{3B^2}\right) I\left(-\frac{A^2}{B^{4/3}}\right). \tag{4.16}$$

Note that, in contrast to formula (2.7), no divergence occurs at $A = 0$. Rearranging the terms and using relation (4.9) one can write the above expression in a more suggestive way:

$$\Psi_{\mathrm{sc}} = \frac{\mathrm{e}^{-\pi\mathrm{i}/4}}{\sqrt{\pi}}\frac{A^{1/2}}{B^{1/3}}\exp\left(\mathrm{i}\frac{2A^3}{3B^2}\right) I\left(-\frac{A^2}{B^{4/3}}\right) \times \frac{1}{b^{1/2}\pi^{1/4}}\frac{\exp\{\mathrm{i}F(x_0')/\hbar\}}{\sqrt{m_{qq}+\mathrm{i}m_{qp}}}. \tag{4.17}$$

The first term involves only powers of $\zeta \equiv A^{1/2}/B^{1/3}$ and the second one is exactly ψ_{sc}, so that the above formula factorizes into

$$\Psi_{\mathrm{sc}}(x,T) = \chi(\zeta)\psi_{\mathrm{sc}}(x,T), \tag{4.18}$$

with

$$\chi(\zeta) \equiv \frac{\mathrm{e}^{-\pi i/4}}{\sqrt{\pi}}\zeta\exp\left(\mathrm{i}\frac{2\zeta^6}{3}\right) I(-\zeta^4). \tag{4.19}$$

This way of writing Ψ_{sc} makes the role of χ clear. It is a correction which, by consistency, must be relevant only in the vicinity of the caustics, where $\zeta \approx 0$ and ψ_{sc} fails to describe the quantum wavefunction. More precisely:

(a) On the caustics Ψ_{sc} must be bounded. By inspection of equation (4.16) we see that this requirement is indeed satisfied.
(b) Far from the influence region of the caustics we must have $\Psi_{sc} \to \psi_{sc}$. In this regime, $|\zeta| \propto |A^{1/2}| \gg 1$ (if $B \neq 0$). So we have to impose

$$\chi \to 1 \qquad \text{for} \qquad |\zeta| \to \infty (B \neq 0). \tag{4.20}$$

In terms of the integral $I(-\zeta^4)$ we must have

$$I(-\zeta^4) \sim \mathrm{e}^{\pi \mathrm{i}/4} \sqrt{\pi} \zeta^{-1} \exp\left(-\mathrm{i}\frac{2\zeta^6}{3}\right) \qquad \text{if} \qquad \zeta \to \infty, \tag{4.21}$$

which follows directly from definition (4.19). At this point, we still have two problems to cope with. First, we must choose one of the six possible contours $\pm\mathcal{C}_j$ for each x. Since the structure of valleys and hills of the integrand in (4.14) depends on x through ζ, there is no reason for the contour to be the same for all positions x. Second, given the correct contour we must be careful in choosing the physically consistent branches that appear in the asymptotic expansion of χ.

Let us start with the second problem by assuming that we know the correct contour of integration. Given the contour we must keep only the branches of χ that satisfy the condition (4.20). Let us initially suppose that $I(-\zeta^4) = \pm 2\pi \mathrm{Ai}(-\zeta^4)$, i.e., let us assume that $\mathcal{C} = \pm\mathcal{C}_1$. Since $2\pi \mathrm{Ai}(s) \sim \sqrt{\pi} s^{-1/4} \exp(-2s^{3/2}/3)$ for $s \to \infty$ if $\arg(s) \neq \pi$ [Olv74, Ble86], we can write

$$2\pi \mathrm{Ai}(-\zeta^4) \sim \sqrt{\pi}[(-\zeta^4)^{1/2}]^{-1/2} \exp\left(-\frac{2[(-\zeta^4)^{1/2}]^3}{3}\right) \qquad \text{for} \qquad \zeta \to \infty, \tag{4.22}$$

if $\arg(-\zeta^4) \neq \pi$. With the convenient choice of roots

$$(-\zeta^4)^{1/2} = -\mathrm{i}\zeta^2 \Rightarrow [(-\zeta^4)^{1/2}]^3 = \mathrm{i}\zeta^6 \qquad \text{and} \qquad [(-\zeta^4)^{1/2}]^{-1/2} = \pm \mathrm{e}^{\mathrm{i}\pi/4} \zeta^{-1}, \tag{4.23}$$

we get the right limit (4.20). As we remarked, there is no reason *a priori* for this identification to be the right choice in all cases. In fact, we can immediately verify that it is insufficient because it leads to $\chi \neq 1$ in the limit $\zeta \to \infty$ when ζ^4 is real and positive. Now we recall that

$$\begin{cases} 2\pi f_2(s) \sim -\mathrm{i}\sqrt{\pi} s^{-1/4} \exp(2s^{3/2}/3) \\ 2\pi f_3(s) \sim \mathrm{i}\sqrt{\pi} s^{-1/4} \exp(2s^{3/2}/3) \end{cases} \tag{4.24}$$

for $s \to \infty$. It is easy to show that if we take $I(-\zeta^4) = 2\pi f_2(-\zeta^4)$ or $I(-\zeta^4) = 2\pi f_3(-\zeta^4)$ we also obtain the correct limit, provided that $(-\zeta^4)^{1/2} = \mathrm{i}\zeta^2 \Rightarrow [(-\zeta^4)^{1/2}]^3 = -\mathrm{i}\zeta^6$ and $[(-\zeta^4)^{1/2}]^{-1/2} = \pm \mathrm{e}^{-\mathrm{i}\pi/4} \zeta^{-1}$. We stress that all these previous identifications are possible since the only change from one particular f_j to another is the contour of integration, with the integrand in (4.13) remaining unchanged. All possibilities must be taken into account in order to satisfy the condition (4.20) for all values of x. If we keep the choice of roots fixed by (4.23), we can write the correction factor as

$$\chi(\zeta) = \begin{cases} +2\sqrt{\pi}\, \mathrm{e}^{-\pi \mathrm{i}/4} \zeta \exp(\mathrm{i}2\zeta^6/3) \mathrm{Ai}(-\zeta^4) & \text{if} \quad \mathcal{C} \sim \pm\mathcal{C}_1 \\ +2\sqrt{\pi}\, \mathrm{e}^{\pi \mathrm{i}/4} \zeta \exp(-\mathrm{i}2\zeta^6/3) f_2(-\zeta^4) & \text{if} \quad \mathcal{C} \sim \pm\mathcal{C}_2 \\ -2\sqrt{\pi}\, \mathrm{e}^{\pi \mathrm{i}/4} \zeta \exp(-\mathrm{i}2\zeta^6/3) f_3(-\zeta^4) & \text{if} \quad \mathcal{C} \sim \pm\mathcal{C}_3. \end{cases} \tag{4.25}$$

All we have to do now is to select one of the expressions above for each x. This, of course, corresponds to the choice of the correct contour that must be made through a careful analysis of the topology of the complex action along with the determination of the relevant steepest descent contours (see subsection 5.5 and section 6).

5. Application: wave packet bouncing off a smooth wall

In this section, we study in detail the semiclassical scattering of a Gaussian packet by the potential

$$V(x') = \frac{1}{x'^2}, \tag{5.1}$$

which represents a smooth wall that goes to infinity at $x' = 0$ (see [Man96] for a calculation involving real trajectories). This potential is also the centrifugal part of the effective potentials appearing in the radial equations of central force problems. The classical trajectories for this potential can be obtained analytically, which enable us to obtain explicit expressions for the semiclassical wavefunctions ψ_{sc} and Ψ_{sc} in terms of the contributing families in the w-plane. Despite the simplicity of the system, it presents both noncontributing trajectories and caustics, together with a peculiar topology in the complex plane of the action function because of the singularity of the potential at $x' = 0$.

5.1. Classical solution

The solution of the equations of motion for $x' > 0$ is given by

$$x'_T = \sqrt{\frac{2T^2}{x'^2_0} + (p'_0 T + x'_0)^2}. \tag{5.2}$$

Using equations (2.9) this can also be written as

$$x'^2_T(w) = \frac{2T^2}{(q+w)^2} + [(p + \mathrm{i}kw)T + (q+w)]^2. \tag{5.3}$$

Note that we can work with either $x'^2_T(w)$ or $x'_T(w)$, since both mappings $w \longrightarrow x'_T(w)$ and $w \longrightarrow x'^2_T(w)$ have the same geometrical structure in the region $\mathrm{Re}\big[x'^2_T(w)\big] \geqslant 0$.

The function $x'^2_T(w)$ is analytic everywhere, except at the isolated singular point $w = -q$. The condition $\mathrm{Im}[x'_T(w)] = 0$ is equivalent to

$$\mathrm{Im}\big[x'^2_T(w)\big] = 0 \qquad \text{and} \qquad \mathrm{Re}\big[x'^2_T(w)\big] \geqslant 0, \tag{5.4}$$

where

$$\mathrm{Re}\big[x'^2_T(w)\big] = \left[(KT + R)^2 - (k\alpha T + \beta)^2 + \frac{2T^2(R^2 - \beta^2)}{(R^2 + \beta^2)^2}\right], \tag{5.5}$$

$$\mathrm{Im}\big[x'^2_T(w)\big] = 2\left[(KT + R)(k\alpha T + \beta) - \frac{2T^2\beta R}{(R^2 + \beta^2)^2}\right], \tag{5.6}$$

$k = c/b$, $R = q + \alpha$ and $K = p - k\beta$.

In our numerical calculations, we have placed the wave packet at $q = 2.0$ with $p = -0.5$ and $b = 0.8$. We also set $\hbar = 0.3 \Rightarrow c \approx 0.37$ and $k \approx 0.47$ (arbitrary units). A natural time scale for this problem is given by the classical turning time of a particle with initial position q and initial momentum p:

$$\mathcal{T} = -\frac{q^3 p}{2 + q^2 p^2}. \tag{5.7}$$

With our choice of parameters, we get $\mathcal{T} \approx 1.33$.

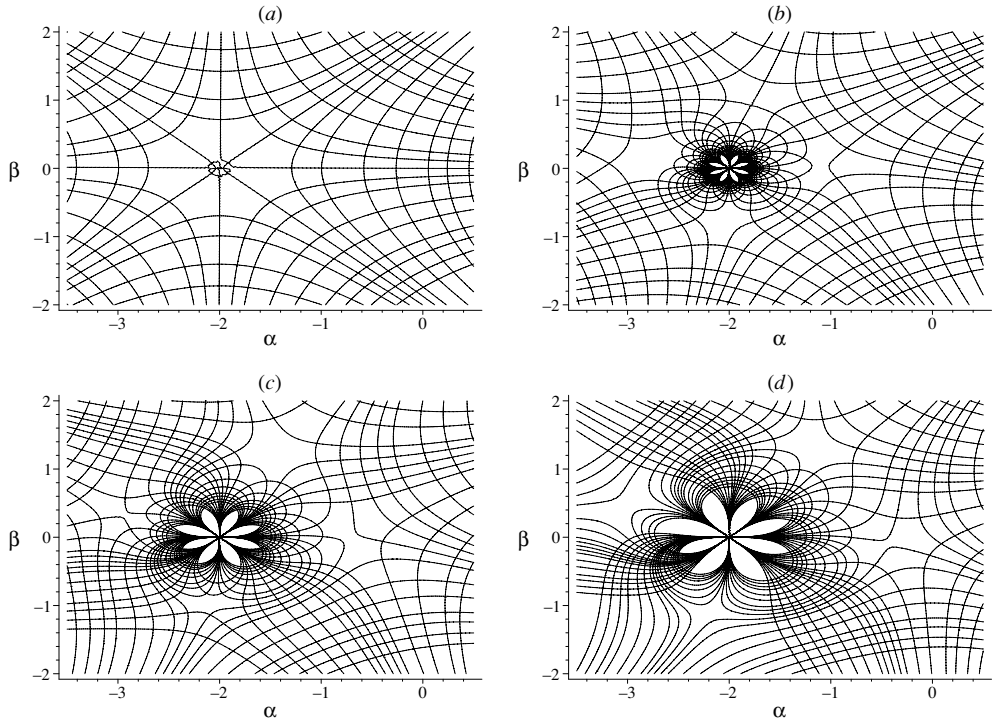

Figure 4. Curves of $\mathrm{Re}[x_T'^2] = \text{const}$ and $\mathrm{Im}[x_T'^2] = \text{const}$ for the propagation times: (*a*) $T = 0.01$, (*b*) $T = 0.5$, (*c*) $T = 1.0$ and (*d*) $T = 1.5$. The four caustics are distinguishable as defects in the reticular pattern. Their approximate coordinates in (*d*) are $(-3.0, 0.4)$, $(-2.2, -1.1)$, $(-1.2, 1.3)$ and $(-0.5, -0.1)$. The flower-like central structure is due to strong oscillations around the singular point $(-2, 0)$.

5.2. *Caustics*

The mapping $w \longrightarrow x_T'(w)$ is conformal except at the singular point and at the caustics. The number and dynamic properties of these points in the present system are quite distinct from the previous ones studied in the literature [Ada89, Rub95]. The critical points are given by $\mathrm{d}x_T'(w)/\mathrm{d}w = 0$, i.e.,

$$(q+w)^3[(1+\mathrm{i}kT)w + pT + q] = \frac{2T^2}{1+\mathrm{i}kT}, \qquad w \neq -q. \tag{5.8}$$

There are, therefore, only four caustics in the w-plane for all values of $T \neq 0$ (see figure 4). When $T = 0$ this equation becomes simply $(q+w)^4 = 0$ which tells us that these points do not come from infinity as in most cases [Rub95] but from the singular point $w = -q$. This makes the effect of the caustics appear very soon in the wave packet propagation. On the other hand, in the limit $T \to \infty$ the same equation reads $(q+w)^3(p - \mathrm{i}kw) = 2/\mathrm{i}k$, that is, the caustics tend to a static configuration in the w-plane. This static configuration depends on (q, p) and on the ratio $k = c/b$. All these features can be seen in figure 4 where curves of constant value of $\mathrm{Re}\big[x_T'^2(w)\big]$ and $\mathrm{Im}\big[x_T'^2(w)\big]$ are shown for different times. Figure 4(*a*) shows the initial stage with $T = 0.01$. Note that, except by the immediate vicinity of the singular point, the arrangement of lines is completely regular. The lines cross at right angles due to the conformal property of the mapping (2.10). For $T = 0.5$ (figure 4(*b*)) the pattern is more

complicated and a flower-like structure appears, revealing the strong oscillations around the singular point. The four caustics are clearly distinguishable as defects in the reticular pattern in figures 4(*c*) and (*d*) for $T = 1.0$ and $T = 1.5$, respectively.

5.3. Complex action and tangent matrix

The complex action S can also be calculated explicitly and is given by

$$S = \tfrac{1}{\sqrt{2}}[Q(T) - Q(0)] - \sqrt{2}\tan^{-1}[Q(T)] + \sqrt{2}\tan^{-1}[Q(0)], \tag{5.9}$$

where

$$Q(t) = \frac{\sqrt{2}}{2}\left[\left(\frac{2}{x_0'^2} + p_0'^2\right)t + x_0' p_0'\right]. \tag{5.10}$$

In order to identify the contributing and noncontributing solutions it is convenient to separate S in real and imaginary parts. After some algebra, we get

$$\begin{aligned}\mathrm{Re}[S] = {} & \frac{1}{2}\left[K^2 - k^2\alpha^2 + \frac{2(R^2-\beta^2)}{(R^2+\beta^2)^2}\right]T \\ & - \frac{\sqrt{2}}{2}\tan^{-1}\left[\frac{2\,\mathrm{Re}[Q(T)]}{1-|Q(T)|^2}\right] + \frac{\sqrt{2}}{2}\tan^{-1}\left[\frac{2\,\mathrm{Re}[Q(0)]}{1-|Q(0)|^2}\right],\end{aligned} \tag{5.11}$$

and

$$\begin{aligned}\mathrm{Im}[S] = {} & \left[k\alpha K - \frac{2\beta R}{(R^2+\beta^2)^2}\right]T - \frac{\sqrt{2}}{2}\ln\left[\frac{\sqrt{(1-|Q(T)|^2)^2 + 4(\mathrm{Re}[Q(T)])^2}}{1+|Q(T)|^2 - 2\,\mathrm{Im}[Q(T)]}\right] \\ & + \frac{\sqrt{2}}{2}\ln\left[\frac{\sqrt{(1-|Q(0)|^2)^2 + 4(\mathrm{Re}[Q(0)])^2}}{1+|Q(0)|^2 - 2\,\mathrm{Im}[Q(0)]}\right].\end{aligned} \tag{5.12}$$

In the above expressions, the branches were chosen such that $S = 0$ for $T = 0$. The elements m_{qq} and m_{qp} of the tangent matrix can be obtained from the variation of x_T':

$$\delta x_T' = \frac{1}{x_T'}\left(p_0' T + x_0' - \frac{2T^2}{x_0'^3}\right)\delta x_0' + \frac{T}{x_T'}(p_0' T + x_0')\delta p_0'. \tag{5.13}$$

We obtain

$$m_{qq} + \mathrm{i}m_{qp} = \frac{1}{x_T'}\left[(p_0' T + x_0')(1 + \mathrm{i}kT) - \frac{2T^2}{x_0'^3}\right]. \tag{5.14}$$

As expected, by setting $m_{qq} + \mathrm{i}m_{qp} = 0$, we recover the caustic equation (5.8).

5.4. The semiclassical wavefunction

Replacing the action and tangent matrix into equation (2.7), we get

$$\psi_{\mathrm{sc}} = \frac{\pi^{-1/4} b^{-1/2} x^{1/2}}{\sqrt{(p_0' T + x_0')(1 + \mathrm{i}kT) - 2T^2/x_0'^3}} \exp\{-\mathrm{Im}[F]/\hbar\} \exp\{\mathrm{i}\,\mathrm{Re}[F]/\hbar\} \tag{5.15}$$

where we have set $x_T' = x$, see (2.8), and

$$\mathrm{Re}[F] = \mathrm{Re}[S] + p\left(R - \frac{q}{2}\right) - \frac{\hbar\alpha\beta}{b^2}, \tag{5.16}$$

and

$$\mathrm{Im}[F] = \mathrm{Im}[S] + p\beta + \frac{\hbar}{2b^2}(\alpha^2 - \beta^2). \tag{5.17}$$

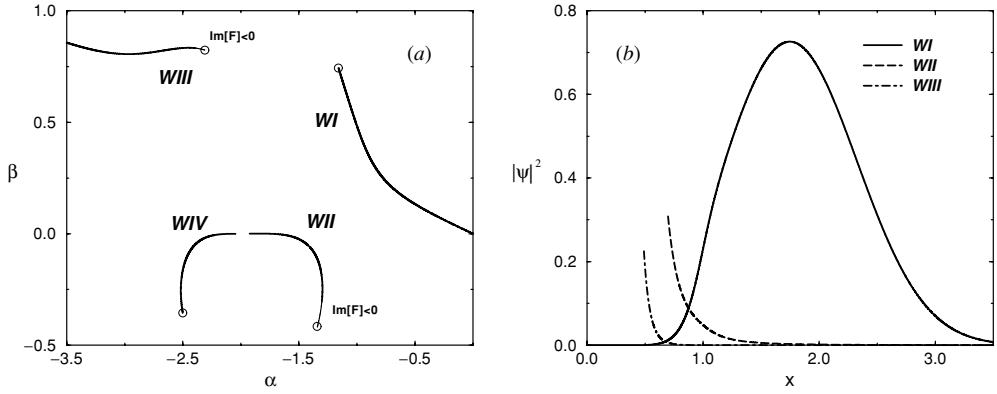

Figure 5. (*a*) Contributing families for $T = 0.5$. The open circles mark the location of the points which are mapped into $x'_T = x = 0$. The thin lines have $\mathrm{Im}[F] < 0$. In (*b*), we show the individual contributions of WI, WII and WIII to the semiclassical wavefunction. Note that no interference appear in these isolated functions.

Equation (5.15) also depends on x implicitly through the contributing families, which can be regarded as parametric curves with x as the parameter. Note that $\psi_{\mathrm{sc}} \to 0$ for $x \to 0$ as expected.

In order to apply formula (5.15) we have to solve equations (5.4) to get the curves in the w-plane which correspond to trajectories satisfying the proper boundary conditions. There are four such families, which we label by WI, WII, WIII and WIV. These families are shown in figure 5(*a*) for $T = 0.5$. We call WI the main family [Agu05] because it contains the real trajectory through the point $(\alpha, \beta) = (0, 0)$. As pointed out by Adachi [Ada89], we must define an allowed region in the w-plane and restrict the computation of the semiclassical propagator to the contributing families which are inside this region. Roughly speaking, this procedure corresponds to the elimination of the inadmissible saddle points that frequently appear in stationary phase calculations. In the allowed region the following properties have to be satisfied:

(i) Trajectories with $\mathrm{Im}[F] < 0$ must be removed. This avoids divergence of $\exp\{-\mathrm{Im}[F]/\hbar\}$ in the limit $\hbar \to 0$ [Ada89].
(ii) Trajectories with $\mathrm{Im}[F_J](x) > 0$ but $\mathrm{Im}[F_J(x)] < \mathrm{Im}[F_I(x)]$ (where $J = \mathrm{II}, \mathrm{III}, \mathrm{IV}$) also have to be removed to guarantee that, as $\hbar \to 0$, the main family always gives the dominant contribution [Agu05].
(iii) The discontinuity introduced by the sudden removal of a secondary contribution must be minimized [Ada89].

Figure 5(*a*) shows that WII and WIII have parts where $\mathrm{Im}[F] < 0$ (shown with a thin line). These intervals cannot be considered in the semiclassical calculations. In fact, criteria (ii) and (iii) make the noncontributing intervals extend into regions of $\mathrm{Im}[F] > 0$. Note that all families shown in figure 5 in the w-plane are mapped into the whole parametric x interval $(0, +\infty)$. However, while families I and III are semi-infinite, WII and WIV occupy only a small limited region in the w-plane. The open circles correspond to points mapped into $x'_T = x = 0$. In figure 5(*b*), we show the individual contributions of WI, WII and WIII to the semiclassical wavefunction (5.15). The main family gives the most important quantitative contribution, WII and WIII give small but still relevant contributions, while WIV is negligible. Note that the wavefunction computed with a single contribution does not show interference

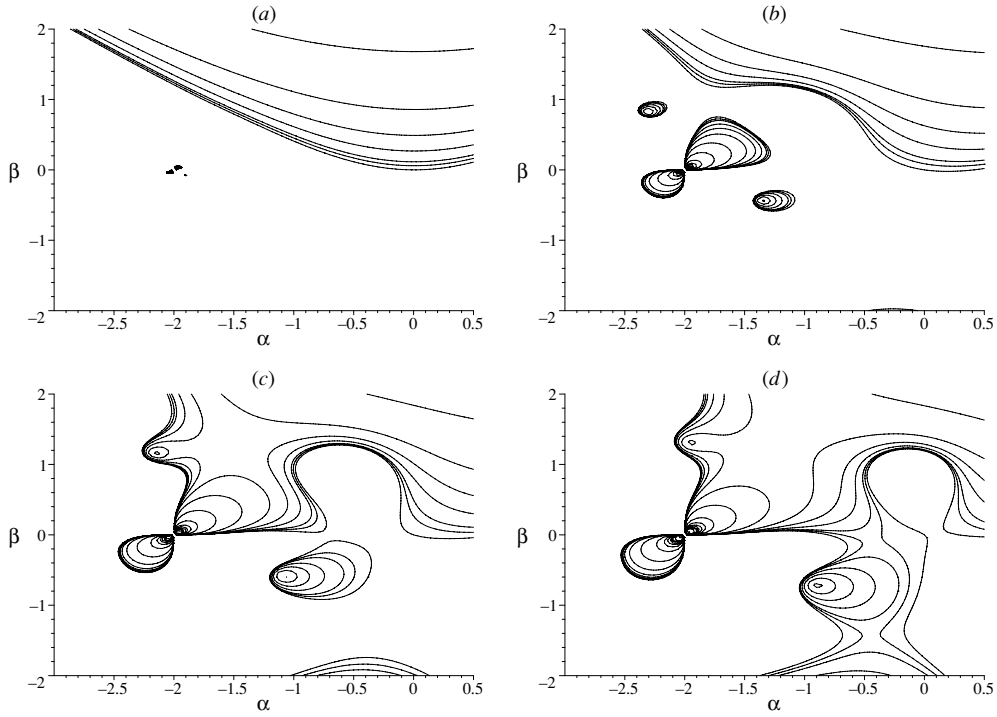

Figure 6. Curves $\mathrm{Im}[F] = \text{const} < 0$ for (*a*) $T = 0.01$, (*b*) $T = 0.5$, (*c*) $T = 1.0$ and (*d*) $T = 1.5$. Note that in (*a*), besides the large forbidden regions, there are also small forbidden regions surrounding the singular point. These initially small regions expand in (*b*) and then coalesce in (*c*) and (*d*), where two disconnected allowed regions can be seen. The family I lies on the right region, whereas all other families are on the left-hand side.

patterns. In the next subsection, we shall show an explicit example of the integration contour being deformable so as to include the family WII in the 'allowed region' but not outside it.

Figure 6 shows the regions where $\mathrm{Im}[F] \leqslant 0$ for the same times as in figure 4. We remark that even for very early propagation times (figure 6(*a*)), there are forbidden regions around the singular point $w = -2.0$. This is a signature of the presence of the caustics that originate from this point. These initially small regions expand (figure 6(*b*)) and as time goes by they coalesce to form the pattern displayed in figures 6(*c*) and (*d*). This pattern also tends to a static configuration for $T \gg \mathcal{T}$.

Once we have found the four families and evaluated their individual contributions, we proceed to compute their composition in order to get ψ_{sc}. In figure 7(*a*), we display the initial wave packet. In figures 7(*b*)–(*d*) we show the semiclassical and exact quantum mechanical (denoted by ψ_{qm}) evolution of the initial packet for different times. In particular, the result displayed in figure 7(*b*) is the composition of the contributions shown in figure 5(*b*). The accuracy of formula (2.7) is very good for $T = 0.5$ and $T = 1.0$, where one can see the interference pattern of the quantum mechanical result precisely reproduced semiclassically. As a general rule, we observe that interference appears in the semiclassical formula only through the combination of the individual contributions. It is worth noting that the normalization $\mathcal{N}$ of the semiclassical wavefunction is very good in figure 7(*b*) ($\mathcal{N} \approx 1.000$) and figure 7(*c*)

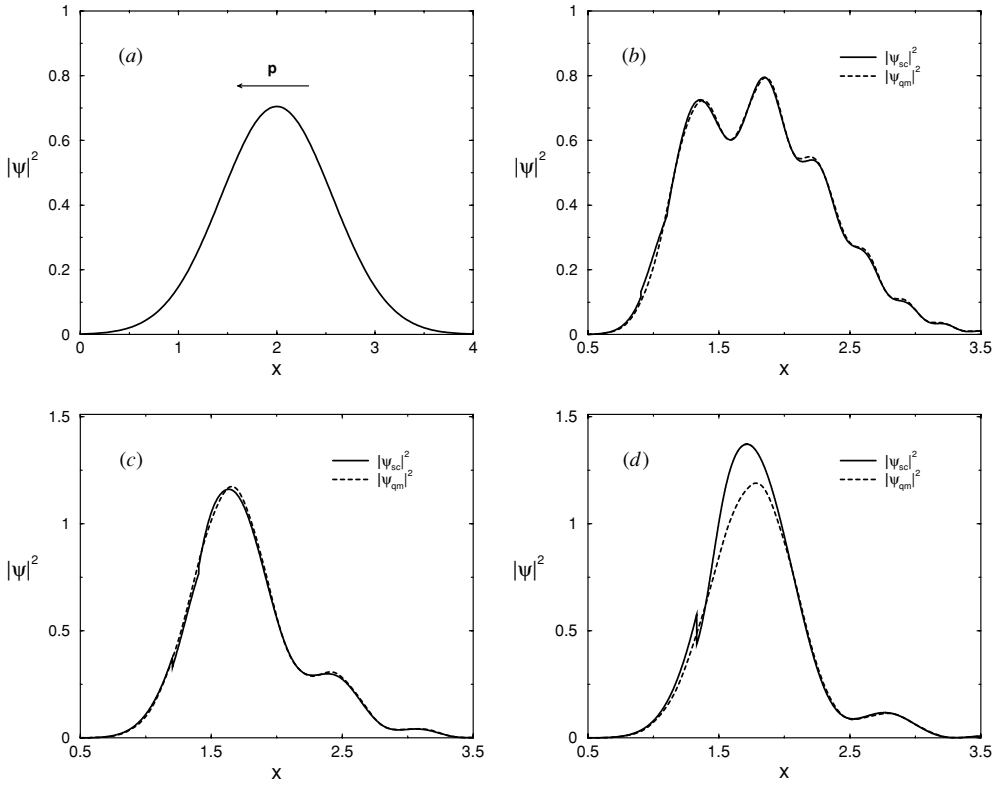

Figure 7. Exact (dashed line) and semiclassical (full line) probability densities for (*a*) $T = 0$, (*b*) $T = 0.5$, (*c*) $T = 1.0$ and (*d*) $T = \mathcal{T} = 1.33$. The semiclassical results are very accurate in (*b*) and (*c*), but the effect of the caustic located between the families I and II considerably decreases its accuracy in (*d*).

($\mathcal{N} \approx 0.987$). For $T \gtrsim \mathcal{T}$, the increase in the pre-factor due to the caustics causes a worsening in the normalization of the semiclassical result, as can be seen in figure 7(*d*), where $T = \mathcal{T} = 1.33$ and $\mathcal{N} \approx 1.092$. Similar effects can be observed in figure 9 of [Hub88] and also in figures 4(*c*) and (*d*) of [Agu05].

5.5. *Steepest descent contours and Stokes phenomenon*

So far we have used criteria (i)–(iii) to decide on the inclusion or elimination of a particular family in the semiclassical formula. In this subsection, we shall carry out an analysis of the saddle point evaluation of integral (4.1). With the help of the Klauder–Adachi mapping we have calculated complex trajectories with given initial conditions (x'_0, p'_0). Now, in order to determine the van Vleck kernel, we must satisfy the boundary conditions $x'(0) = x'$ and $x'(T) = x$. From the classical solution

$$x'(T) = \sqrt{\frac{2T^2}{x'^2} + (p'(0)T + x')^2}, \tag{5.18}$$

it follows that

$$p'_{\pm}(0) = -\frac{x'}{T} \pm \frac{1}{Tx'}\sqrt{x^2x'^2 - 2T^2} \equiv -\frac{x'}{T} \pm \frac{1}{Tx'}\sqrt{\mathcal{Y}}. \tag{5.19}$$

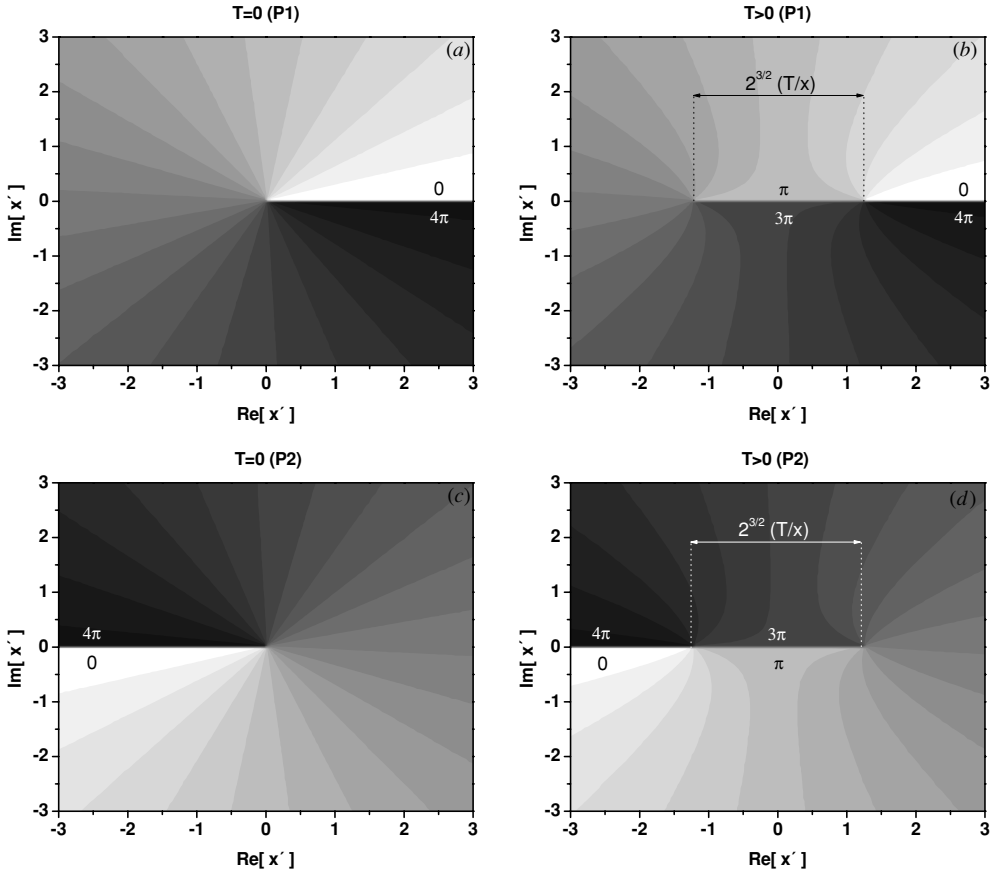

Figure 8. Phases of $\mathcal{Y}$ in $P1$ for $T = 0$ (a) and $T > 0$ (b), and $P2$ for $T = 0$ (c) and $T > 0$ (d). The colours vary from black to white as the phase changes from 4π to 0.

Therefore, there are two initial momenta which are compatible with the van Vleck boundary conditions. From expression (1.1), we see that equation (4.1) is in fact a sum of two integrals whose exponents F must be evaluated for the two corresponding signs in equation (5.19). The saddle point evaluation of these integrals requires an analytic extension of x' to the complex plane $x' \to \mathrm{Re}[x'] + \mathrm{i}\,\mathrm{Im}[x']$. We call the complex x'-planes where these two integrations take place $P1$ and $P2$, respectively. In order to avoid discontinuities in the complex momentum we have to define the phase of $\mathcal{Y}$ modulo 4π, due to the square root in equation (5.19). To do so we note that $\mathcal{Y} = x^2 x'^2$ for $T = 0$. This implies that points in the x'-plane with $\mathrm{Im}[x'] > 0$ correspond to $\arg(\mathcal{Y})$ in the interval $(0, 2\pi]$ and points with $\mathrm{Im}[x'] < 0$ lead to $\arg(\mathcal{Y})$ in the interval $(2\pi, 4\pi]$. The phase of $\mathcal{Y}$ for $T = 0$ is shown in the x'-plane in figure 8(a) for the positive root and in figure 8(c) for the negative root (which can be obtained by adding 2π to the phase of $\mathcal{Y}$). Of course, the $0 \leftrightarrow 4\pi$ jumps do not lead to any discontinuity in $\sqrt{\mathcal{Y}}$. Figures 8(b) and (d) show $\arg(\mathcal{Y})$ for $T > 0$. The situation is now different, since a branch cut develops, leading to a $\pi \leftrightarrow 3\pi$ jump and causing an abrupt change in the sign of $\sqrt{\mathcal{Y}}$. The continuity of sing requires changing sheets $P1 \leftrightarrow P2$. Therefore, the overall structure of the complex plane leads to a continuous variation of the exponent F provided one changes sheets when crossing the branch cut segment, given

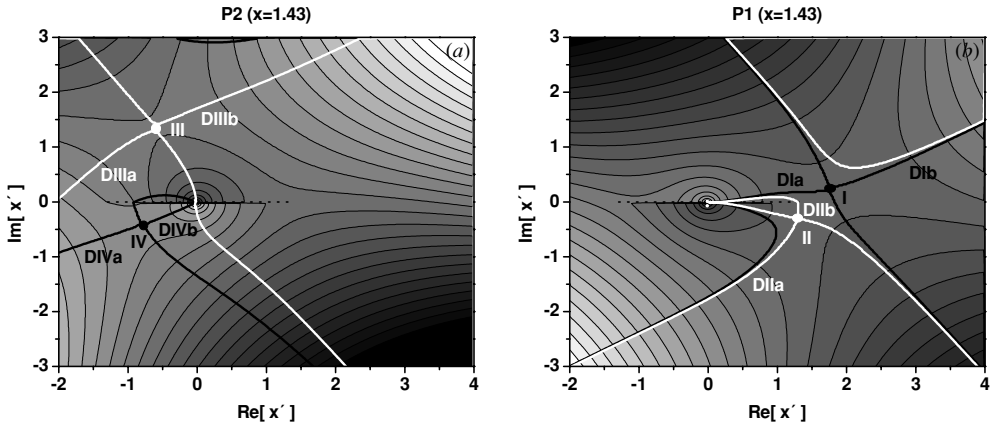

Figure 9. Contour plot of $-\mathrm{Im}[F]$ for $x = 1.43$ and $T = 1.33$ in $P2$ (a) and $P1$ (b). The cutting segment is shown by dotted line. Darker regions correspond to larger positive values and lighter regions to larger negative values.

by the real interval $[-\sqrt{2}T/x, \sqrt{2}T/x]$. The exponent $F(x, T; x', 0)$, equation (4.2), with $S = [Q(T) - Q(0)]/\sqrt{2} - \sqrt{2}\tan^{-1}[Q(T)] + \sqrt{2}\tan^{-1}[Q(0)]$, is also defined in $P1 + P2$. This can be seen explicitly by expressing $Q(t)$ in terms of x and x':

$$Q(0) = \frac{1}{\sqrt{2}T}(-x'^2 \pm \sqrt{\mathcal{Y}}), \qquad Q(T) = \frac{1}{\sqrt{2}T}(x^2 \mp \sqrt{\mathcal{Y}}). \tag{5.20}$$

Once we know the topological structure of $P1 + P2$ we can address the question of sudden removal of secondary families in the wavefunction. As an example, we consider the removal of family II for $T = \mathcal{T} = 1.33$ (corresponding to figure 7(d)), around the point $x = 1.33$. In figure 9, we present contour plots of $-\mathrm{Im}[F]$ for $x = 1.43$ and $T = 1.33$, where WII still contributes to ψ_{sc}. We show valleys (lighter regions) and hills (darker regions) along with the steepest ascent and steepest descent (labelled by the capital letter D) contours passing through each saddle point. We see that points III (white) and IV (black) belong to $P2$ (figure 9(a)) and points I (black) and II (white) belong to $P1$ (figure 9(b)). Since the potential is infinite for $x' = 0$ and the initial wave packet is centred at $x' = q = 2$ it is not surprising that the points for which $x' > 0$ (I and II) give the most relevant contributions. Since we have two integrations one must choose the contours that are deformable into two real lines. One of them is DIIIa + DIIIb (in $P2$) which is responsible for the inclusion of III (figure 9(a)), and the other is DIIa + DIIb + DIa + DIb (in $P1$) justifying the inclusion of II and I (figure 9(b)).

Let us now study the same contour plots for $x = 1.23$ and $T = 1.33$, where WII is no longer included in the semiclassical calculation according to criteria (i)–(iii). This configuration is depicted in figure 10. The picture in $P2$ is quite similar to the previous case and we still have III included in the calculation of the semiclassical wavefunction via DIIIa + DIIIb, as shown in figure 10(a). In $P1$, things look different because the branch cut segment (shown in dotted line) is traversed by DIIb, which means that the upper part of this curve, with $\mathrm{Im}[x'] > 0$, must be placed in $P2$. It turns out that the upper part of DIIb is a steepest *ascent* line in $P2$, since in this sheet the divergence at the origin is positive for $\mathrm{Im}[x'] \to 0^+$ and negative for $\mathrm{Im}[x'] \to 0^-$, the inverse occurring in $P1$. Therefore, DIIb can no longer be regarded as a valid contour of integration. This means that II must not be included in the calculation of ψ_{sc}. The second real line is now deformable in DIVa + DIVb + DIa + DIb (in $P2$ and $P1$). This is a manifestation of the so-called Stokes phenomenon, namely, the

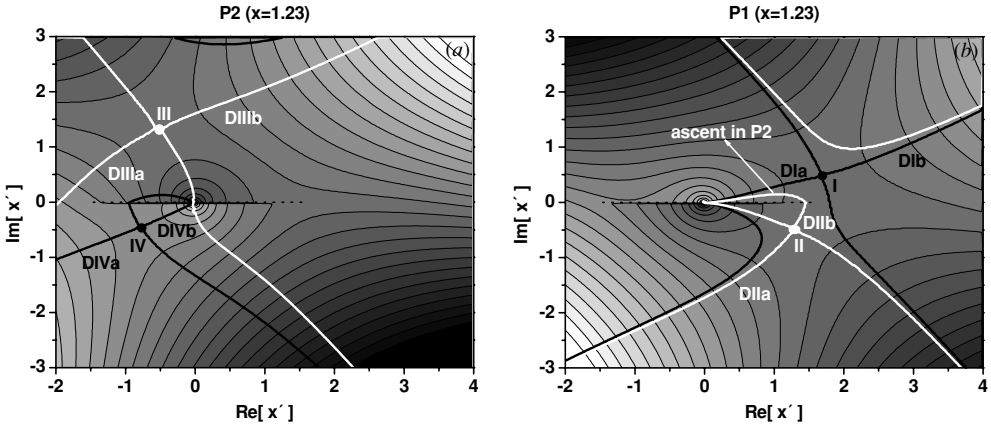

Figure 10. Contour plot of $-\mathrm{Im}[F]$ for $x = 1.23$ and $T = 1.33$ in $P2$ (a) and $P1$ (b). The cutting segment, shown by dotted line, is crossed by DIIb. Darker regions correspond to larger positive values and lighter regions to larger negative values.

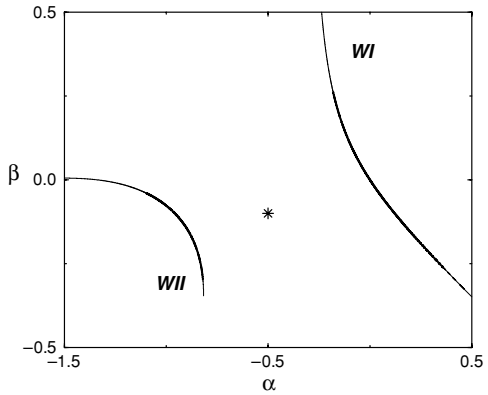

Figure 11. Parts of families I and II that correspond to the region in which the bare semiclassical formula fails. The location of the caustic is marked with a star.

sudden removal of a saddle point due to a smooth change in the geometry of the exponent (F) caused by a continuous variation of some parameter (in the present case x). Later we shall see that this phenomenon plays an important role in the correct determination of Ψ_{sc}, the regular semiclassical wavefunction.

5.6. Regular approximation

Now we will show that the discrepancy between the exact and semiclassical results in figure 7(d) is indeed due to the caustic located between families I and II. We note that in that figure the region where the semiclassical formula fails is given approximately by $1.4 < x < 2.0$. This interval in the position x corresponds to the intervals in the α–β plane shown in figure 11 with thick lines, along with the location of the caustic, represented by a star. From this panel, it is clear that the spurious effects introduced in the bare semiclassical approximation are caused by the presence of the caustic. We can also verify that the contribution of WIII is not affected by the presence of any of the four caustics. Furthermore,

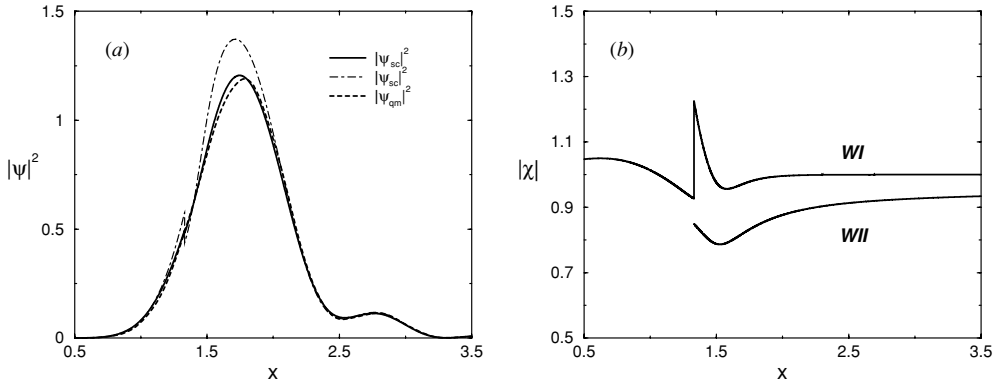

Figure 12. (*a*) Probability densities for $T = \mathcal{T} = 1.33$ (see figure 7(*d*)). The corrected semiclassical result (full line) is very close to the exact one (dashed line). The 'bare semiclassical' result is also shown with a dotted–dashed line. Part (*b*) shows the modulus of the correction factor χ as a function of x for families I and II.

the distance between the families has the same magnitude of $B^{-1/3}$, so we apply formula (4.18) only to the contributions of WI and WII, the contribution of the third family remaining unchanged. To apply equation (4.18), we need to calculate $\zeta = A^{1/2}/B^{1/3}$. For the smooth wall, we get the explicit expressions

$$A = \frac{1}{2\hbar T(p_0' T + x_0')}\left[(p_0' T + x_0')(1 + \mathrm{i}kT) - \frac{2T^2}{x_0'^3}\right], \tag{5.21}$$

and

$$B = \frac{T(3p_0' T + 4x_0')}{\hbar x_0'^4 (p_0' T + x_0')^2}. \tag{5.22}$$

Figure 12(*a*) shows the results obtained with the corrected formula (full line). The 'bare semiclassical' (dotted–dashed line) and quantum mechanical (dashed line) results are also displayed. We have used the numerical routines in [Amo01] for the computation of the Airy functions. The improvement obtained with equation (4.18) is very significant, specially where formula (5.15) causes a nonphysical increase in the probability density. The normalization of the wavefunction with the corrected formula becomes $\mathcal{N} \approx 1.003$. As expected, far from this region both semiclassical formulae give very similar results. This is due to the property (4.20), which can be seen to hold in figure 12(*b*) where we plot the modulus of χ as a function of x. Note that for WI the correction factor rapidly tends to unity, while for WII there is a saturation around $|\chi| \approx 0.94$. This is because WII occupies a small region in the vicinity of the caustic. So, for this family, even points that are mapped into $x \gg 1$ are close to the caustic in the w-plane. It is worth noting that the discontinuity introduced by the removal of WII is virtually cancelled by the discontinuity that comes from the change in the type of Airy function entering in the calculation of χ for WI. This might look mysterious at first glance, but it is another manifestation of the same Stokes phenomenon we studied in the last section. Since χ is a local correction, in order to choose the proper contour out of the six possibilities $\pm\mathcal{C}_j$ it is necessary to analyse the steepest descent lines in the vicinities of the saddle point I (for which χ presents the discontinuity) and compare them to the curves $\mathcal{C}_j$ that arise from the expansion of F. In figure 13, we plot the expanded function $-\mathrm{Im}[F]$, as given by (4.7), from which we can infer the positions of $\mathcal{C}_j$ relative to the relevant steepest descent contours. The discontinuity of χ for the family I can now be understood. Before the removal of II the

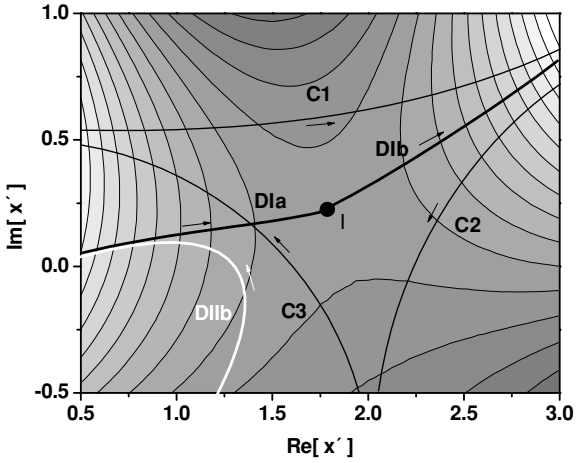

Figure 13. Contour plot of the third-order expansion of $-\mathrm{Im}[F]$. The contours $\mathcal{C}_j$ are shown together with the steepest descents around the saddle point I. The removal of DIIb leads to the transition $-\mathcal{C}_2 \to \mathcal{C}_1$. Darker regions correspond to larger positive values and lighter regions to larger negative values.

contour in the neighbourhood of I is DIIb + DIa + DIb (see figures 9(*b*) and 13) that is clearly deformable into $\mathcal{C}_3 + \mathcal{C}_1$ which, by Cauchy's integral theorem, is equivalent to $-\mathcal{C}_2$. When II is eliminated DIIb is not a valid contour and only DIa + DIb remains as the correct contour in the vicinity of I, being deformable into $\mathcal{C}_1$. This explains why the change in the contour of the Airy function for family I coincides with the removal of family II.

It is important to note that the consistency condition (4.20) imposes a limitation to the validity of the expression (4.18). This condition says that $\chi \to 1$ as $\zeta \to \infty$. So, if $|A| \gg 1$, i.e., if the caustics are far from the relevant region, the correction must be negligible. However, we must note that $\zeta \to \infty$ also if $B \propto F''' \to 0$, which not necessarily occurs far from the caustics. Therefore, expression (4.18) becomes ill defined at the points where $A = 0$ and $B = 0$ simultaneously. These points correspond to higher order caustics, causing the semiclassical formula (4.18) to fail in their neighbourhood. For the system we are studying, there is one point in which $B = 0$ ($w \neq -2.0$) whose coordinates are

$$\alpha = -\frac{q + 3pT/4}{1 + (3kT/4)^2} \qquad \text{and} \qquad \beta = \frac{2kT}{4}\frac{q + 3pT/4}{1 + (3kT/4)^2}. \tag{5.23}$$

For $T = 0$ it coincides again with the singular point $w = -q$. For $T \to \infty$, it tends towards $w = (0, 2p/3k)$ and does not seem to affect the results very much.

6. Concluding remarks

The semiclassical propagation of Gaussian wave packets with complex trajectories involves the calculation of multiple classical paths satisfying some specific boundary conditions. In between these several trajectories there are phase space caustics, special points at which the semiclassical formula diverges. Although these points do not generally lie on the paths entering in the semiclassical formula, their effect might be important, causing spurious peaks in the propagated wave packet.

In this, paper we have derived an improved third-order semiclassical expression for the propagation of Gaussian wave packets that is well behaved in the vicinity of these phase space

caustics. Its application, though perhaps less general, is simpler than that of the uniform approximation. The regular approximation can be written as the product of a correction function χ by the usual second-order semiclassical formula $\psi_{\rm sc}$. This reduces the problem to the determination of χ, which involves the Airy function (or the associated functions f_2 and f_3) of a complex argument.

Our semiclassical formula was applied to the case of a Gaussian wave packet under the influence of the repulsive potential $V(x) = 1/x^2$. Unlike most systems previously studied in the literature, we found a finite number of caustics and contributing trajectories. This indicates that the proliferation of complex classical solutions, which is not limited to chaotic dynamics [Rub95], is closely related to propagation in confining potentials. The bare semiclassical results have proved to be very accurate within the range of applicability of the theory. However, as the wave packet approaches the smooth wall, i.e., for T close to the time of the classical turning point, the second-order semiclassical wavefunction starts to display a nonphysical peak in the probability density. This peak is removed by the application of our formula, equation (4.18). The calculation of the correction function χ involves the choice of a path of integration, which might change discontinuously. For the example studied in section 5 this happens when the steepest descent path associated with a secondary family of complex trajectories collides with a branch cut that develops in the complex plane. This collision eliminates the contribution of that family and at the same time changes the contour of integration of the correction factor χ. The resulting semiclassical wavefunction improves considerably the bare approximation, achieving very good agreement with the exact quantum calculations.

Acknowledgments

The authors gratefully acknowledge Dr A D Ribeiro for valuable suggestions and discussions. This work was partly supported by the Brazilian agencies FAPESP (contracts 01/05746-3 and 04/13525-5) and CNPq.

Appendix A. Transitional formula

We now present the corrected formula that arises when the expansion of the effective action is made around the caustic. The mathematical procedure is similar to that presented in this paper, thus we only give the main steps towards the final expression. The expansion of F reads

$$F(x,T;x',0) \approx F(x'_c) + F'(x'_c)(x'-x'_c) + \tfrac{1}{6}F'''(x'_c)(x'-x'_c)^3, \tag{A.1}$$

since $F''(x'_c) = 0$. The transitional semiclassical wavefunction can be expressed as

$$\Psi_{\rm sc}^{(c)}(x,T) = \frac{{\rm e}^{-{\rm i}\pi/4}\exp\{{\rm i}F(x'_c)/\hbar\}}{b^{3/2}\pi^{1/4}\sqrt{2\pi m_{qp}}}\int_{\mathcal{C}}\exp\left\{{\rm i}F'(x'-x'_c)+\frac{{\rm i}F'''}{6}(x'-x'_c)^3\right\}{\rm d}x'. \tag{A.2}$$

With the transformation of coordinates $t = (F'''/2\hbar)^{1/3}(x'-x'_c)$, we get

$$\Psi_{\rm sc}^{(c)}(x,T) = \frac{{\rm e}^{-{\rm i}\pi/4}\exp\{{\rm i}F(x'_c)/\hbar\}}{b^{3/2}\pi^{1/4}\sqrt{2\pi m_{qp}}}\left(\frac{2\hbar}{F'''}\right)^{1/3} I\left[\left(\frac{2F'^3}{\hbar^2F'''}\right)^{1/3}\right], \tag{A.3}$$

where $I(s)$ is given by definition (4.14). In the above expression it is not possible to factorize $\psi_{\rm sc}$ as we did in section 4. Furthermore, $\Psi_{\rm sc}^{(c)}$ must be calculated on classical trajectories starting at $x'(0) = x'_c$ and ending at $x'(T) = x$ and therefore, differently from the regular formula, the paths that contribute to the determination of $\Psi_{\rm sc}^{(c)}$ *are not* the same as the ones

that enter in the calculation of ψ_{sc}. As before, these classical paths must be chosen from a detailed analysis of the steepest descent contours. Expression (A.3) is expected to give good results only in the vicinity of the caustics and must be replaced by ψ_{sc} out of this region.

Appendix B. Consistency of definitions (4.12)

In this appendix, we study more closely the change of variables given by (4.11) and the choice of roots made in equations (4.12). We must note that relation (4.11) remains valid for any choice of roots in equation $\gamma^3 = B$. Therefore, we have the following possible relations:

$$\gamma = e_j B^{1/3}, \qquad \sigma = \frac{A}{e_j^2 B^{2/3}}, \qquad \mu = -\frac{A^2}{e_j^4 B^{4/3}} = -\frac{A^2}{e_j B^{4/3}}; \tag{B.1}$$

with

$$e_j = \mathrm{e}^{(2\pi \mathrm{i}/3)j} \qquad \text{for} \quad j = 0, +1, -1. \tag{B.2}$$

In this paper, we have chosen $j = 0$, see equation (4.12), and we concluded that $\chi \propto I(-\zeta^4)$. However, there must not be a special choice and the physical result must be the same independently of j. It is easy to show that in the general case we have

$$\chi \propto e_{-j} I[e_{-j}(-\zeta^4)]. \tag{B.3}$$

There is another modification introduced by a different choice of roots because the angle between the axes of x' and t is given by $\arg(\gamma)$ since (see the text after equation (4.12))

$$x' = \gamma^{-1} t + \text{const.} \tag{B.4}$$

Now, suppose we choose the root $j = 0$ and find, for example, the contour of integration to be $\mathcal{C}_2$. Then we would conclude that $\chi \propto f_2(-\zeta^4)$. Now, let us take a different choice, say $j = 1$. From relation (B.4) we see that this implies an extra counterclockwise (x' fixed) rotation between the axes of x' and t by an angle of $2\pi/3$. In this case, we would find that the integration contour would be $\mathcal{C}_1$, which together with relation (B.3) would lead to $\chi \propto e_{-1} f_1[e_{-1}(-\zeta^4)] = \mathrm{e}^{-2\pi \mathrm{i}/3}\mathrm{Ai}[\mathrm{e}^{-2\pi \mathrm{i}/3}(-\zeta^4)] = f_2(-\zeta^4)$ [Ble86], which is the same result obtained with $j = 0$. This argumentation can be extended to any choice of j demonstrating that the overall result is independent of this choice.

References

[Ada89] Adachi S 1989 A numerical evaluation of the semiclassical coherent state path integral *Ann. Phys.* **195** 45

[Amo01] Amos D E 2001 www.netlib.org/amos

[Agu05] de Aguiar M A M, Baranger M, Jaubert L, Parisio Fernando and Ribeiro A D 2005 Semiclassical propagation of wave packets with complex and real trajectories *J. Phys. A: Math. Gen.* **38** 4645

[Bar01] Baranger M, de Aguiar M A M, Keck F, Korsch H J and Schellhaaß B 2001 Semiclassical approximations in phase space with coherent states *J. Phys. A: Math. Gen.* **34** 7227

[Ber67] Berry M V 1967 Uniformly approximate solutions for short-wave problems *SERC Research Report* available at http://www.phy.bris.ac.uk/research/theory/Berry/publications.html

[Ble86] Bleistein N and Handelsman R A 1986 *Asymptotic Expansions of Integrals* (New York: Dover)

[Fie03] Fiete G A and Heller E J 2003 Semiclassical theory of coherence and decoherence *Phys. Rev.* A **68** 022112

[Hub87] Huber D and Heller E J 1987 Generalized Gaussian wave packet dynamics *J. Chem. Phys.* **87** 5302

[Hub88] Huber D, Heller E J and Littlejohn R G 1988 Generalized Gaussian wave packet dynamics, Schrödinger equation, and stationary phase approximation *J. Chem. Phys.* **89** 2003

[Kay05] Kay K G 2005 Semiclassical initial value treatments of atoms and molecules *Annu. Rev. Phys. Chem.* **56** 255

[Kla85] Klauder J R and Skagerstam B S 1985 *Coherent States, Applications in Physics and Mathematical Physics* (Singapore: World Scientific)

[Kla79] Klauder J R 1979 Path integrals and stationary-phase approximations *Phys. Rev.* D **19** 2349
[Man96] Manning R S and Ezra G S 1996 Uniform regularized semiclassical propagator for the x^{-2} potential *Phys. Rev.* A **53** 661
[Olv74] Olver F W J 1974 *Asymptotics and Special Functions* (New York: Academic)
[Oni01] Onishi T, Shudo A, Ikeda K S and Takahashi K 2001 Tunneling mechanism due to chaos in a complex phase space *Phys. Rev.* E **64** 025201
[Pro95] Provost D and Brumer P 1995 Uniform semiclassical wave-packet propagation and eigenstate extraction in a smooth chaotic system *Phys. Rev. Lett.* **74** 250
[Rib04] Ribeiro A D, de Aguiar M A M and Baranger M 2004 Semiclassical approximations based on complex trajectories *Phys. Rev.* E **69** 066204
[Rib05] Ribeiro A D, Novaes M and de Aguiar M A M 2005 Uniform approximation for the coherent-state propagator using a conjugate application of the Bargmann representation *Phys. Rev. Lett.* **95** 050450
[Rub95] Rubin A and Klauder J R 1995 The comparative roles of connected and disconnected trajectories in the evaluation of the semiclassical coherent-state propagator *Ann. Phys.* **241** 212
[Shu95] Shudo A and Ikeda K S 1995 Complex classical trajectories and chaotic tunneling *Phys. Rev. Lett.* **74** 682
[Shu96] Shudo A and Ikeda K S 1996 Stokes phenomenon in chaotic systems: pruning trees of complex paths with principle of exponential dominance *Phys. Rev. Lett.* **76** 4151
[Sil02] Silvestrov P G and Beenakker C W J 2002 Ehrenfest times for classically chaotic systems *Phys. Rev.* E **65** 035208
[Tho04] Thoss M and Wang H B 2004 Semiclassical description of molecular dynamics based in initial-value representation methods *Annu. Rev. Phys. Chem.* **55** 299
[Tom91] Tomsovic S and Heller E J 1991 Semiclassical dynamics of chaotic motion—unexpected long-time accuracy *Phys. Rev. Lett.* **67** 664
[Tom03] Tomsovic S and Heller E J 2003 Comment on 'Ehrenfest times for classically chaotic systems' *Phys. Rev.* E **68** 038201